This is a repository copy of *Mechanisms of vascular damage by systemic dissemination of the oral pathogen Porphyromonas gingivalis*.

White Rose Research Online URL for this paper:
https://eprints.whiterose.ac.uk/164322/

Version: Published Version

Mechanisms of vascular damage by systemic dissemination of the oral pathogen *Porphyromonas gingivalis*

Cher Farrugia[1] (iD), Graham P. Stafford[1], Jan Potempa[3,5], Robert N. Wilkinson[2], Yan Chen[4], Craig Murdoch[1] (iD) and Magdalena Widziolek[1,3,6]

1 School of Clinical Dentistry, University of Sheffield, UK
2 School of Life Sciences, Medical School, University of Nottingham, UK
3 Department of Microbiology, Faculty of Biochemistry, Biophysics and Biotechnology, Jagiellonian University, Kraków, Poland
4 Department of Infection, Immunity and Cardiovascular Disease, Medical School, University of Sheffield, UK
5 Department of Oral Immunity and Infectious Diseases, University of Louisville School of Dentistry, KY, USA
6 Department of Evolutionary Immunology, Institute of Zoology and Biomedical Research, Faculty of Biology, Jagiellonian University, Kraków, Poland

Several studies have shown a clear association between periodontal disease and increased risk of cardiovascular disease. *Porphyromonas gingivalis* (*Pg*), a key oral pathogen, and its cell surface-expressed gingipains, induce oedema in a zebrafish larvae infection model although the mechanism of these vascular effects is unknown. Here, we aimed to determine whether *Pg*-induced vascular damage is mediated by gingipains. *In vitro*, human endothelial cells from different vascular beds were invaded by wild-type (W83) but not gingipain-deficient (ΔK/R-ab) *Pg*. W83 infection resulted in increased endothelial permeability as well as decreased cell surface abundance of endothelial adhesion molecules PECAM-1 and VE-cadherin compared to infection with ΔK/R-ab. In agreement, when transgenic zebrafish larvae expressing fluorescently labelled PECAM-1 or VE-cadherin were systemically infected with W83 or ΔK/R-ab, a significant reduction in adhesion molecule fluorescence was observed specifically in endothelium proximal to W83 bacteria through a gingipain-dependent mechanism. Furthermore, this was associated with increased vascular permeability *in vivo* when assessed by dextran leakage microangiography. These data are the first to show that *Pg* directly mediates vascular damage *in vivo* by degrading PECAM-1 and VE-cadherin. Our data provide a molecular mechanism by which *Pg* might contribute to cardiovascular disease.

Introduction

The effect of oral health on systemic disease is currently a highly debated topic with increasing evidence indicating that blood-borne oral microbes significantly contribute to conditions such as cardiovascular disease (CVD) [1,2], rheumatoid arthritis [3], diabetes [4] and Alzheimer's disease [5]. The association between periodontitis and cardiovascular disease has been studied for the last three decades and is now generally accepted in the field [6].

Periodontitis is a chronic multifactorial inflammatory disease caused by the dysbiosis of indigenous

Abbreviations

CVD, cardiovascular disease; HCAEC, human primary coronary artery endothelial cells; HDMEC, human dermal microvascular endothelial cells; HMEC, human microvascular endothelial cells; ICAM, intercellular adhesion molecule; PECAM, platelet endothelial cell adhesion molecule; *Pg, Porphyromonas gingivalis*; VE, vascular endothelial.

microorganisms and characterised by the destruction of tooth-supporting structures leading to tooth loss [7,8]. *Porphyromonas gingivalis* (*Pg*), an oral anaerobic microbe, is considered the keystone pathogen that promotes the development of severe periodontitis by favouring oral microbial dysbiosis and dysregulation of the host immune response [9]. *Pg* resides in dental plaque and produces several virulence factors that enable this microbe to colonise the host, evade the immune system and contribute to disease progression and tissue destruction [9,10]. The predominant virulence factors appear to be gingipains, cysteine proteases with significant proteolytic activity [11].

The presence of oral bacteria has been detected in peripheral blood following tooth extractions and even regular oral hygiene procedures such as tooth brushing, giving rise to a transient bacteraemia in healthy individuals [12]. However, the likelihood of bacterial entry to the circulation is greatly increased in patients with chronic gingivitis or periodontitis where bacterial-mediated loss of gingival epithelial integrity facilitates bleeding, allowing pathogenic oral bacteria facile movement from the periodontal pocket into the bloodstream [13–15]. Indeed, oral microbiome profiling performed on patients with atherosclerotic CVD undergoing bypass surgery revealed that *Pg* was the most abundant species found in nondiseased vascular tissue [16]. Furthermore, *Pg* DNA was detected in cardiac valves of patients with CVD and deep periodontal pockets [17].

Pg is able to bind to and invade endothelial cells cultured *in vitro* [18,19]. This microbial–host interaction mediates increased gene expression of several chemokines (e.g. CXCL8, CCL2), adhesion molecules (CD54, CD62E, PECAM-1) and inflammatory factors by endothelial cells via various mechanisms [20–22]. Paradoxically, in an attempt by the pathogen to subvert the host immune response, the proteins of these pro-inflammatory genes are degraded by *Pg*-derived gingipains [20,23,24]. Adhesion molecules localised at the cellular junctions of adjacent endothelial cells selectively regulate vascular permeability [25]. Dysregulated adhesion molecule expression may initiate vascular pathology due to abnormally elevated vascular permeability leading to oedema, chronic inflammatory and vascular damage [26]. We recently showed that *Pg* can cause vascular damage in an *in vivo* zebrafish larvae model of systemic infection in a gingipain-dependent manner [27], suggesting that these bacterial proteases may be important factors in the development of CVD. Here, we hypothesised that gingipain-dependent cleavage of endothelial cell junction adhesion molecules is important in mediating the vascular damage. By infecting transgenic zebrafish models that have fluorescent labelling of endothelial cell junctions with a wild-type and isogenic gingipain-null *Pg* mutant, we identify that gingipains dramatically alter adhesion molecule cell surface abundance leading to increased vascular permeability *in vitro* and *in vivo*. These data significantly enhance the growing evidence for the role of oral bacteria in CVD and indicate a potential mechanism by which oral bacteria can contribute to cardiovascular disease.

Results

P. gingivalis invades human endothelial cells and localises to the perinuclear region through a gingipain-dependent mechanism

We initially confirmed *Pg* invasion of endothelial cells using an antibiotic protection assay. All wild-type laboratory strains examined (ATCC33277, W83, W50) invaded HDMEC at significantly greater levels than the clinical isolate (A245Br) ($P \leq 0.05$, Fig. 1A). Wild-type W83 was not only capable of invading various types of endothelial cells including HDMEC ($0.072\% \pm 0.032$; Fig. 1A,B), HMEC-1 ($0.48\% \pm 0.2$; Fig. 1C) and HCAEC ($0.21\% \pm 0.1$; Fig. 1D), but was also shown to be significantly more invasive than the gingipain-deficient ΔK/R-ab mutant ($P < 0.001$) that displayed on average an 85% reduction in endothelial cell invasion for the three cell types tested (Fig. 1B–D). Multichromatic confocal microscopy revealed that intracellular dwelling *Pg* were predominantly localised to the perinuclear regions, where they were colocalised within wheat germ agglutinin-positive membranes, suggesting residence within membrane-bound intracellular vesicles following internalisation, as previously shown in other model systems (Fig. 1E).

Endothelial cell permeability increases following *Pg* infection and is gingipain-dependent

We previously demonstrated that zebrafish systemically infected with *Pg* displayed significant oedema [27], suggesting that this bacterium may influence vascular permeability. To explore this possibility, we examined HDMEC monolayer permeability following *Pg* infection *in vitro*. Microscopically, *Pg*-infected HDMEC were found to lose cell–cell attachments compared with uninfected controls (Fig. 2A). Using a high molecular weight fluorescent dextran permeability assay, we observed a time-dependent increase in the levels of fluorescence passing through the endothelial monolayer and this was significantly increased in *Pg*-
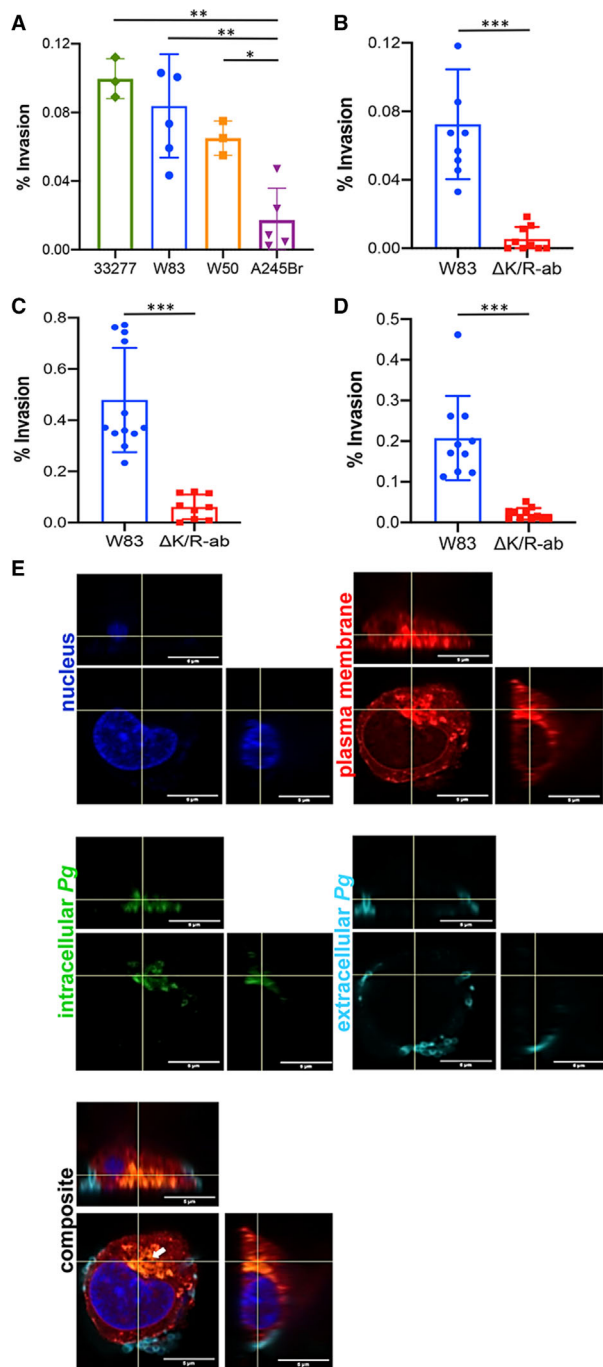
Fig. 1. Strain and gingipain-dependent invasion of *Pg* into human endothelial cells. HDMEC were infected with wild-type strain *Pg* ATCC33277, W83, W50 or A245Br (A) or wild-type *Pg* W83 and ΔK/R-ab (B) at a MOI 100 for 90 min. HMEC-1 (C) and HCAEC (D) were infected with wild-type *Pg* W83 or ΔK/R-ab mutant also at a MOI 100 for 90 min. Bacterial cell invasion was determined by antibiotic protection assay and expressed as a percentage of primary bacterial inoculum recovered. Graphs show means ± SD (*n* = at least 3 individual experiments with each individual experiment performed in triplicate technical repeats; shown as filled circles). Data were analysed using one-way ANOVA with Tukey's post hoc comparison test (Fig. 1A) or Student's *t*-test (Fig 1B-D), *$P < 0.05$, **$P < 0.01$, ***$P < 0.001$. Representative maximum intensity Z projection images of HMEC-1 with intracellular (green) and extracellular (cyan) *Pg* W83. Cell nucleus (blue) and plasma membrane (red). Composite image shows intracellular dwelling *Pg* as orange (green and red colocalisation, white arrow), and extracellular (cyan) bacteria bound to the cell surface (E). All images show *x*-axis, *y*-axis and *z*-axis planes, and scale bars in images are all 5 μm.

were infected with the gingipain-deficient mutant ΔK/R-ab compared with wild-type controls (Fig. 2D). Collectively, these data implicate gingipains as the primary permeabilising factor following *Pg* infection.

Pg infection decreases endothelial cell surface adhesion molecule abundance but not gene expression *in vitro*

The endothelial cell surface adhesion proteins PECAM-1 (CD31) and VE-cadherin (CD144) are crucial for maintaining cell–cell junction integrity and preserving a restrictive endothelial permeability barrier [25,29]. Gingipains have been shown to mediate the proteolytic degradation of several human proteins [20,30]; therefore, we examined whether these proteases were responsible for cleavage of PECAM-1 and VE-cadherin. Flow cytometric analysis revealed that cell surface abundance of PECAM-1 on both HMEC-1 and HDMEC was almost completely abolished upon W83 infection compared with uninfected controls when analysed by both flow cytometry ($P < 0.05$; Fig. 3A,C) and immunofluorescence microscopy (Fig. 3E). In contrast, endothelial cells infected with the gingipain-null mutant, ΔK/R-ab, showed no loss of PECAM-1, displaying levels similar to uninfected controls (Fig. 3A,C). Cell surface abundance of VE-cadherin on both HMEC-1 and HDMEC was reduced by sixfold upon infection with W83 ($P \leq 0.05$; Fig. 3B,D). In contrast, cells infected with ΔK/R-ab displayed VE-cadherin levels similar to those of uninfected controls (Fig. 3B,D). Loss of VE-cadherin was observed predominantly at the cell–cell junctions by confocal microscopy, sites where this protein

treated compared with untreated HDMEC at all time points examined for up to 5 h (Fig. 2B). Moreover, this increase in endothelium permeability was significantly reduced ($P < 0.001$) compared with untreated control levels or when *Pg* W83 was pre-incubated with KYT, a specific inhibitor of gingipain activity (Fig. 2C) [28]. Similarly, endothelial permeability was also significantly reduced ($P < 0.001$) when monolayers
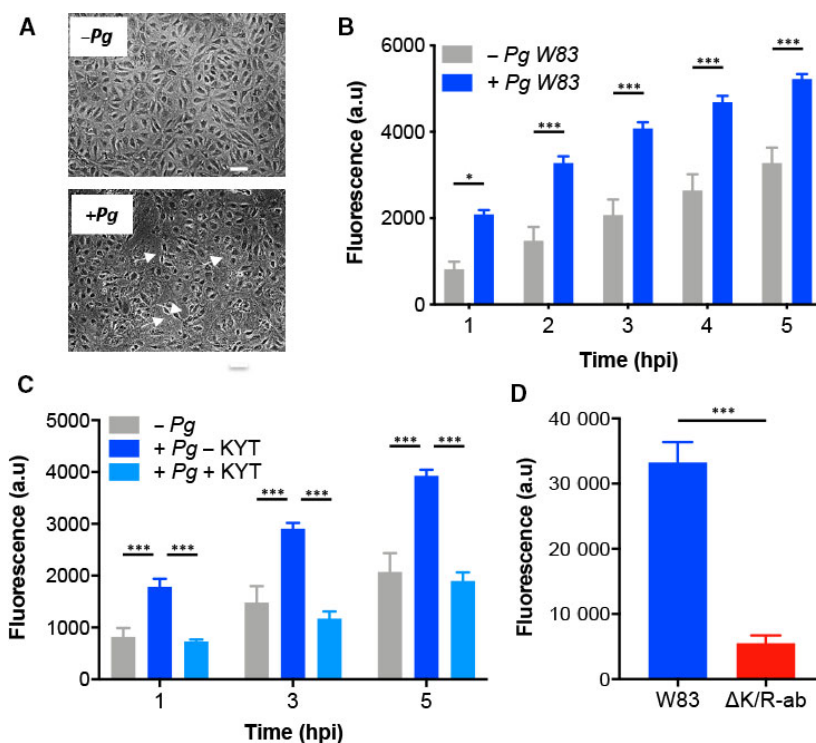
Fig. 2. *Pg* W83 increases permeability of endothelial cell monolayers in a gingipain-dependent manner. HDMEC (A–C) or HMEC-1 (D) cells were grown to confluent monolayers on fibronectin-coated inserts, infected with *Pg* at a MOI 1000 for 1.5 h, followed by the measurement of high molecular weight (70 kDa) fluorescein dextran passing through the monolayer barrier. Morphology of HDMEC monolayer in the absence (−*Pg*) or presence (+*Pg*) of W83 (A); white arrows indicate areas of cell attachment loss (scale bar in A = 20 µm). *In vitro* permeability assay of HDMEC in the absence (−*Pg*) or presence (+*Pg*) of W83 (B) and upon treatment with KYT inhibitors prior to HDMEC *Pg* infection (C). *In vitro* permeability assay of HMEC-1 infected with W83 or ΔK/R-ab (D). Data in B&C are presented as means ± SD and were analysed by one-way ANOVA followed by Tukey's post hoc comparison test. *$P < 0.05$, ***$P < 0.001$. Data in D are presented as means ± SD and were analysed by Student's t-test. ***$P < 0.001$; for all experiments, $n = 3$ individual experiments with each individual experiment performed in triplicate technical repeats.

preferentially accumulates (Fig. 3F). Loss of PECAM-1 adhesion molecule cell surface expression was MOI-dependent (Fig. 4A) and not due to differences in endothelial cell death upon infection as cell viability was similar to controls following infection with either W83 or ΔK/R-ab (Fig. 4B–E). In addition, reduced abundance of the endothelial cell surface adhesion molecule, E-selectin (CD62E), a protein that plays a role in leucocyte adhesion rather than vascular permeability, was also observed (Fig. 5). The levels of cell surface E-selectin were increased on HDMEC at 4 and 8 h following treatment with TNFα, whereas immortalised HMEC-1 cells did not display E-selectin at any time point examined irrespective of cytokine treatment (Fig. 5A–D). *Pg* was able to invade both HDMEC and HMEC-1 at similar levels in the absence or presence of pro-inflammatory stimulation (Fig. 5E,F). In 8-h TNFα-treated HDMEC, infection with *Pg* significantly ($P < 0.001$) reduced E-selectin cell surface abundance by fivefold compared with uninfected controls (Fig. 5G,H).

An alternative explanation for the loss of endothelial cell surface adhesion molecule expression is that the bacterial infection may reduce gene expression. To test for this possibility, we checked for differences in endothelial mRNA expression by qRT–PCR following incubation with wild-type W83 and mutant ΔK/R-ab *Pg*. Incubation with either of these strains did not significantly alter gene expression of *VE-cadherin*, *PECAM-1* or other tested cytokines (*CXCL8, CCL2, ICAM-1*) in HMEC-1 and HDMEC cultures when compared to the treatment with the potent pro-inflammatory cytokine, TNFα (Fig. 6A,B).

P. gingivalis reduces endothelial cell surface adhesion molecule abundance in an *in vivo* zebrafish infection model

We next used our established *Pg* zebrafish infection model [27] to determine whether the observed changes in adhesion molecule cell surface abundance seen *in*
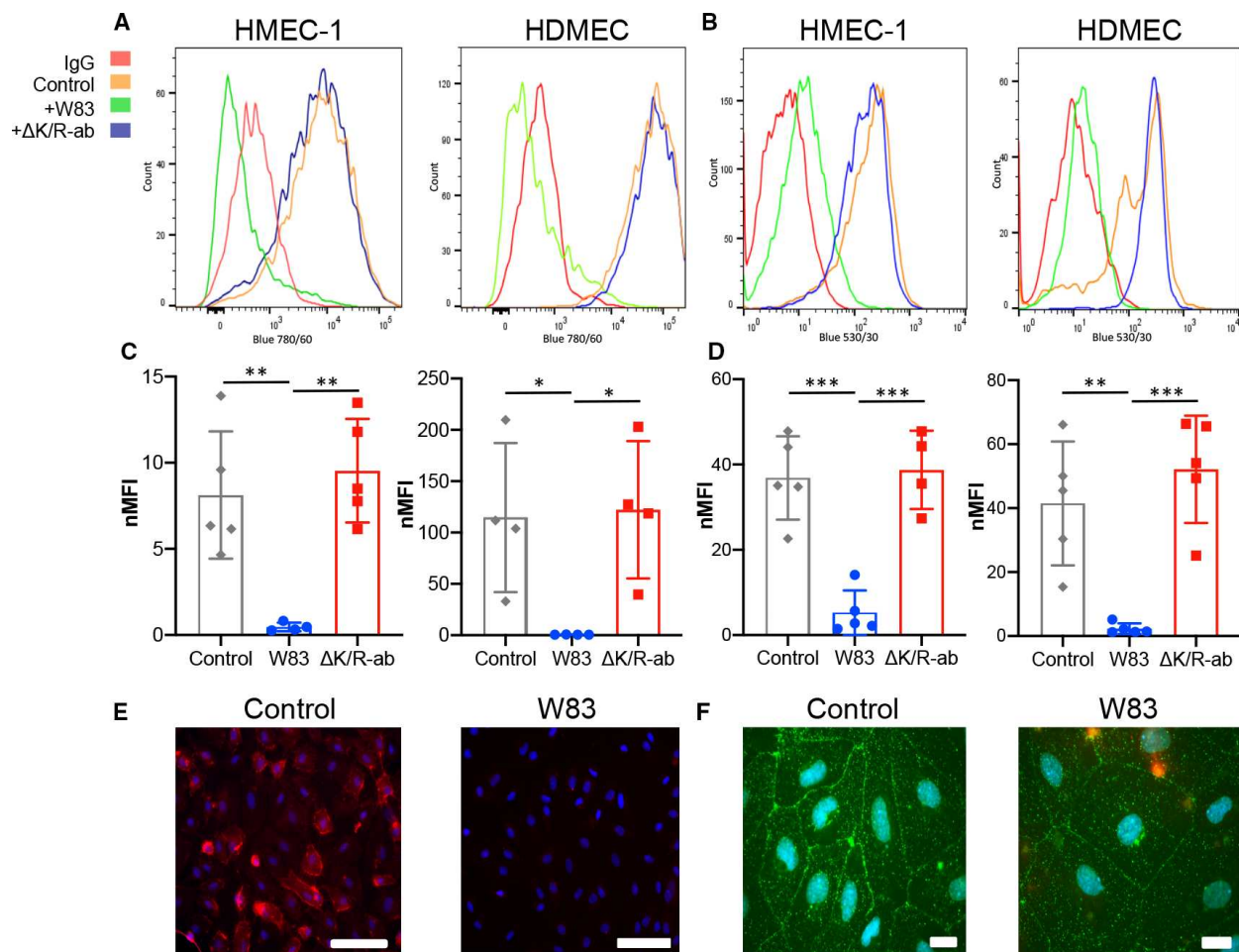
Fig. 3. Degradation of endothelial cell surface-expressed junctional adhesion molecules *in vitro*. Representative flow cytometry histograms of cell surface expression of PECAM-1 (A) and VE-cadherin (B) on HMEC-1 and HDMEC following infection with *Pg* W83 (green) or ΔK/R-ab mutant (blue); IgG control (red); and uninfected control (orange). Normalised median fluorescence intensity (nMFI) histograms of PECAM-1 (C) and VE-cadherin (D) on HMEC-1 and HDMEC following infection with *Pg* W83, ΔK/R-ab or uninfected control (enclosed circles represent data from each individual experiment, $n = 4$). Statistical differences were analysed by one-way ANOVA with Tukey's multiple comparison test *$P < 0.05$, **$P < 0.01$, ***$P < 0.001$. Micrograph images show immunofluorescent detection of cell surface expression of PECAM-1 (red, E) and VE-cadherin (green, F) in control or *Pg*-treated HDMEC ($n = 3$). Nuclei were counterstained blue with DAPI. Scale bars in E & F = 100 μm.

vitro were replicated *in vivo*. Transgenic zebrafish with endothelial cell-specific PECAM-1-EGFP expression *tg (fli1a:PECAM1-EGFP)sh524* were inoculated systemically with either red-labelled wild-type W83 or ΔK/R-ab *Pg*. Reporter fluorescence was quantified where the endothelium and *Pg* colocalised in the intersegmental vessels and the caudal vein adjacent to the yolk sac, anatomical sites that are free from any natural pigmentation to avoid problems with background fluorescence and where individual vessels were easily distinguished. In PBS-injected zebrafish, PCAM-1 expression was observed on the endothelial cell surface of the intersegmental vessels as well as the caudal

artery and vein (Fig. 7A,D). Both W83 and ΔK/R-ab gingipain-null bacteria could be visualised within the vessels at these sites (Fig. 7B,E and C,F), binding to and in some instances having traversed the vascular barrier into surrounding tissue (Fig. 7Gii). Importantly, in W83-infected zebrafish, colocalisation of *Pg* at the endothelial surface was associated with a marked reduction in endothelial PECAM-1 fluorescence at these sites (Fig. 7Gi,Gii). Consistent with our *in vitro* experiments, we observed that loss of PECAM-1-EGFP fluorescence was gingipain-dependent since infection with the gingipain-null mutant, ΔK/R-ab, was not associated with loss of PECAM-1-
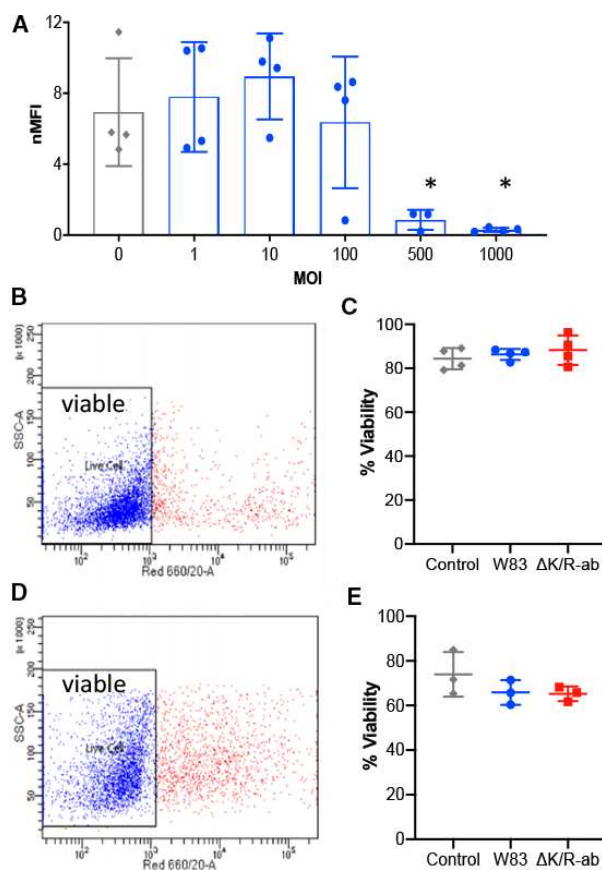
Fig. 4. *Pg*-mediated decrease in PECAM-1 cell surface abundance is MOI-dependent on viable endothelial cells. (A) PECAM-1 cell surface abundance on HMEC-1 cells as determined by flow cytometric analysis following infection with increasing MOI of *Pg*; uninfected cells were used as controls (enclosed circles represent data from each individual experiment). Data are displayed as normalised median fluorescence intensity (nMFI), and statistical differences were analysed by one-way ANOVA with Tukey's multiple comparison test; *$P < 0.05$, **$P < 0.01$ compared with MOI 0, 1, 10. HMEC-1 (B&C) and HDMEC (C&D) viability postinfection as assessed by a live/dead TO-PRO-3 exclusion flow cytometric assay. The level of per cent viable cells (TO-PRO-3-negative, blue dots) in the cell population was measured for W83 and ΔK/R-ab-treated cells. One-way ANOVA with Tukey's multiple comparison test showed no statistically significant differences in cell survival between groups following infection.

EGFP fluorescence (Fig. 7Gi). Indeed, fluorescence intensity analysis showed that PECAM-1 fluorescence was significantly reduced in the presence of W83 compared with ΔK/R-ab on both the intersegmental vessels in the tail (Fig. 7H, $P < 0.001$) and caudal vein (Fig. 7I, $P < 0.01$). We next employed fluorescently tagged VE-cadherin-TS transgenic zebrafish larvae and quantified transgene fluorescence following PBS, W83 or ΔK/R-ab infection (Fig. 8A–F). Similar to the effect

on PECAM1-EGFP, when colocalised with the vasculature (Fig. 8B,Gi), wild-type *Pg* significantly reduced the fluorescence intensity of the VE-cadherin-TS reporter on both intersegmental (Fig. 8H, $P < 0.01$) and caudal vein (Fig. 8I, $P < 0.05$) vessels when compared to ΔK/R-ab mutants, suggesting reduced fluorescence of this reporter fusion protein was also gingipain-dependent.

Pg infection increases vascular permeability *in vivo*

We next tested whether *Pg* infection could also lead to increased vascular permeability in an *in vivo* setting. Here, we used transgenic zebrafish expressing a cyan fluorescent protein, mTurquiose2, in endothelial cells (tg(fli1a:mTQ2)sh321), to fluorescently label the vasculature and injected these with either fluorescein-labelled *Pg* or PBS as control followed by further injection with tetramethylrhodamine (a red fluorescent) dextran at 24 hpi. In PBS-injected larvae, the fluorescent dextran strictly localised to the lumen of the aortic arches, opercular artery, hypobranchial artery and other vessels in the vascular network, indicating that the high molecular weight dextran was not able to pass across the vascular barrier (Fig. 9A,D). Following infection, *Pg* was observed both within blood vessels, their surrounding tissues and in particular around the oedematous heart (Fig. 9B,E). In these infected larvae, diffuse fluorescent dextran staining was observed throughout tissues, extending far beyond the confines of the aortic arches suggesting widespread dextran leakage from vessels (Fig. 9C,F). Furthermore, dextran fluorescence was observed in the oedematous pericardiac region suggesting widespread vessel leakage in this area (Fig. 9C,F). These data, along with our *in vitro* studies, provide compelling evidence that *Pg* is able to mediate vascular damage leading to loss of endothelial integrity and increased vascular permeability.

Discussion

Increasing evidence suggests that periodontal disease is associated with CVD and that this is influenced, in part, by bacteria that enter the circulation via diseased tissues in the oral cavity [1,6]. Further supporting evidence comes from *in vitro* studies showing that oral microbes, in particular *Pg*, can invade endothelial cells, but more compellingly from human studies where the DNA of several oral bacteria, including *Pg*, has been found in nondiseased vascular tissue from patients undergoing bypass surgery [16] as well as in atherosclerotic plaques [31–33]. However, the molecular
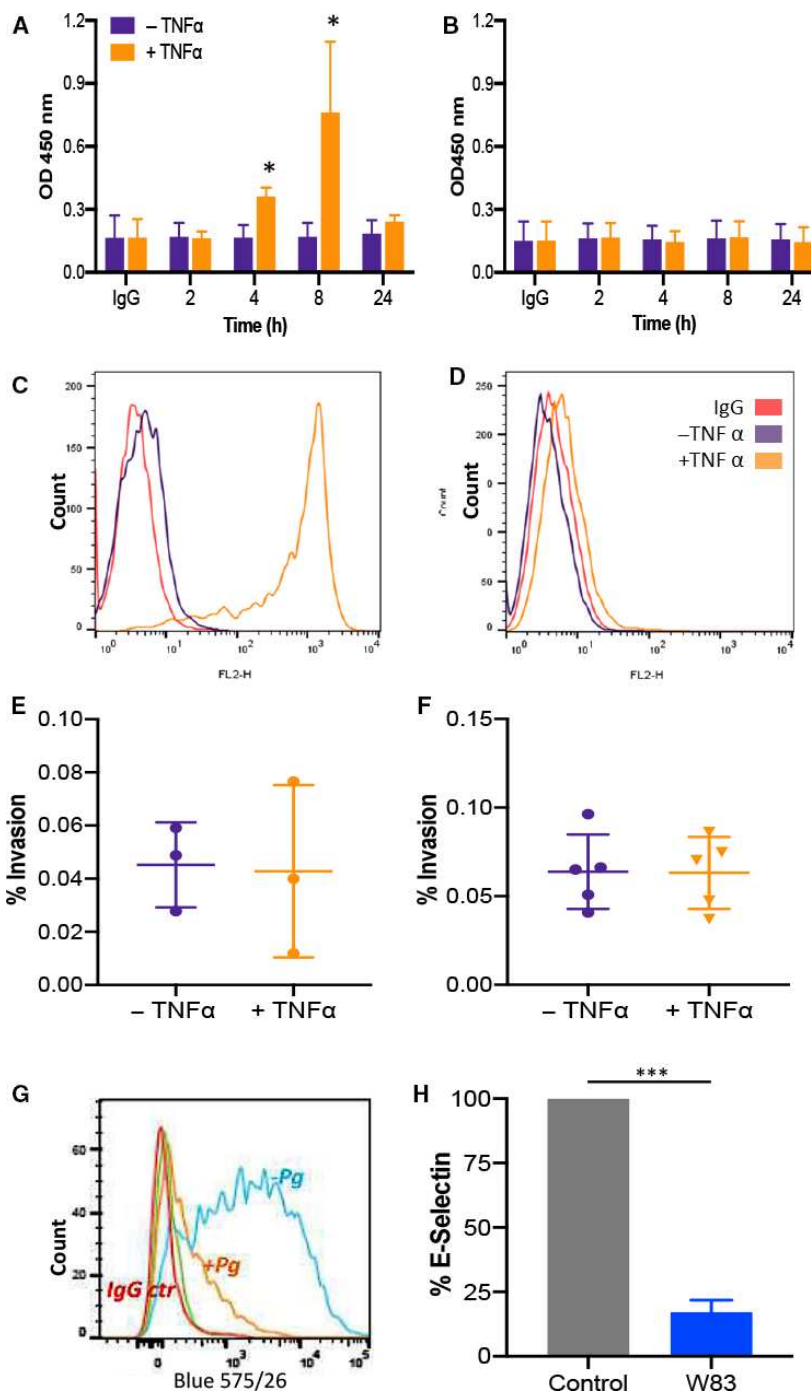
Fig. 5. *Pg W83* infection decreases E-selectin abundance on HDMEC *in vitro*. Cell surface abundance of E-selectin increased in a time-dependent manner on HDMEC (A) upon treatment with TNFα (10 ng·mL⁻¹) when analysed by cell-based ELISA. Expression increased at 4 h, displayed maximal expression after 8 h ($P < 0.05$, Mann–Whitney *U*-test, $n = 3$) with levels returning to baseline by 24 h. HMEC-1 cells did not express E-selectin at any time point examined (B). These data were confirmed by flow cytometric analysis where E-selectin abundance was increased on HDMEC after 8 h TNFα stimulation (C) but was not present on HMEC-1 with levels being similar to unstimulated controls (D). Whisker plots showing that stimulation of HDMEC (E) or HMEC-1 (F) with 10 ng·mL⁻¹ TNFα for 8 h did not result in increased invasion of *Pg* W83 compared with unstimulated control cells (enclosed squares and circles denote number of experiments performed, and data are mean ± SD). Representative flow cytometry histogram of cell surface expression of E-selectin (G) on 8 h TNFα-stimulated HDMEC following infection with *Pg* W83 (orange), IgG control (red) and uninfected control (blue). E-selectin normalised median fluorescence intensity (nMFI) histograms of *Pg* W83-infected and *Pg* W83-uninfected controls. Statistical differences in E, F and H were analysed by Mann–Whitney U-test of $n = 3$ independent experiments, ***$P < 0.001$.

mechanism driving this association is, as yet, unknown, with several divided theories proposed on how this relationship develops. Therefore, in this study we used both *in vitro* and *in vivo* approaches to decipher the mechanisms at play with particular emphasis on the role of gingipains, potent proteases known to play a key role in *Pg*-mediated disease processes [34].

Our initial *in vitro* studies using monolayers of endothelial cells from various vascular beds showed that *Pg* (strains ATCC33277, W83, W50, A245Br) were invasive but at low levels (~ 0.1%), which is in agreement with previous findings from other groups [18,19,35,36]. Collectively, these data show that endothelial cells are less susceptible to invasion than
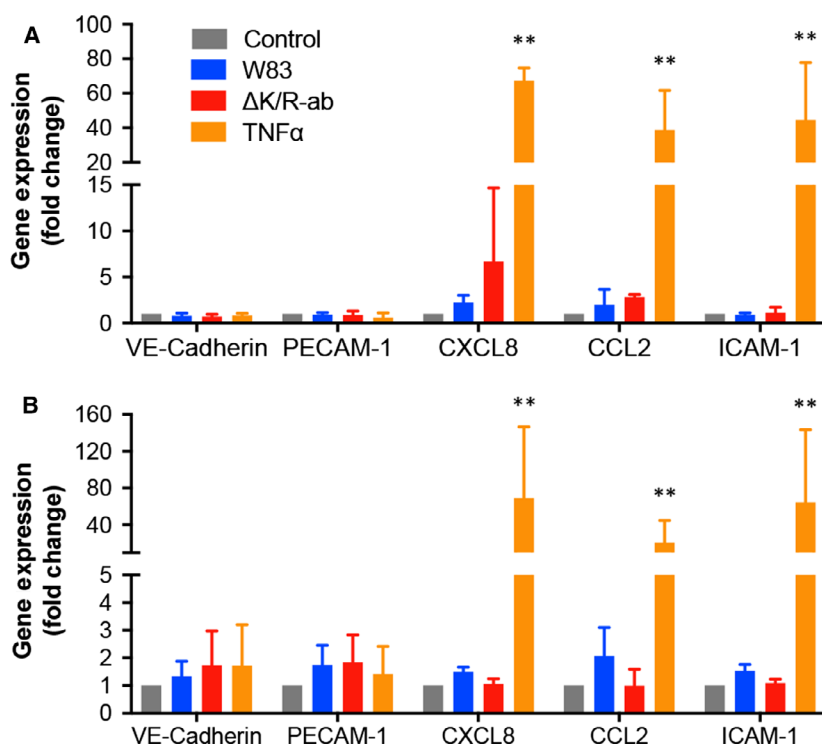
Fig. 6. Infection of endothelial cells with *Pg* W83 or ΔK/R-ab does not alter mRNA expression of pro-inflammatory genes. HMEC-1 (A) and HDMEC (B) cells were infected with either W83 or ΔK/R-ab (MOI 100) for 4 h, unstimulated or TNFα-stimulated (25 ng·mL^{-1}) cells were used as controls. Bars represent means ± SD of relative fold change expression of VE-cadherin, PECAM-1, CXCL8, CCL2 and ICAM-1. Data were analysed by Kruskal–Wallis with Dunn's multiple comparison test; **$P \leq 0.01$, $n = 3$ individual biological experiments each performed in triplicate technical repeats.

oral epithelial keratinocytes that can display from 2% to 10% cell invasion depending on the strain examined [37,38]. Moreover, the gingipain-null mutant ΔK/R-ab failed to invade endothelial cells, suggesting that bacterial gingipains are crucial for this process. Confocal microscopy analysis confirmed the presence of intracellular dwelling *Pg* enclosed within membrane-bound vesicles at perinuclear sites in endothelial cells, similar to that documented for gingival epithelial cells, most likely as a result of endocytosis [19,39,40]. Internalisation has several beneficial outcomes for the bacterium including protection from the host immune response, resistance to antibiotic therapy (many cannot pass the plasma membrane) and increased survival [39]. When infected with wild-type *Pg*, HDMEC within confluent monolayers became detached and the endothelium displayed significant loss of permeability *in vitro* that was prevented by inhibition of gingipain enzyme activity or upon infection with ΔK/R-ab, the gingipain-null strain. Similar observations were reported by Sheets *et al.* [24] who noted that bovine coronary artery endothelial cells and HDMEC exhibited loss of adhesion to tissue culture plastic upon culture with *Pg*-derived culture extracts. These data clearly point to proteolytic degradation of cell surface molecules as the likely mechanism for loss of cell–cell contacts and adhesion. Indeed, our flow cytometric and confocal microscopy analysis revealed gingipain-dependent

cleavage of PECAM-1, VE-cadherin and E-selectin (CD62E) on human endothelial cells when cultured as monolayers *in vitro*.

E-selectin is an adhesion molecule associated with tethering of leucocytes to the endothelium during inflammation. It was previously shown that *Pg* adhesion to human umbilical vein endothelial cells (HUVEC) that are derived from large blood vessels is mediated by E-selectin [24,41]. In contrast, our data indicate that *Pg* adhere and invade both E-selectin-deficient HMEC-1 and E-selectin-expressing HDMEC at similar levels, suggesting that E-selectin is not essential for invasion into microvascular endothelial cells. Gingipain-dependent degradation of other leucocyte adhesion molecules (ICAM-1/CD54, VACM-1/CD106) has also been observed [30], suggesting that *Pg* is able to modulate leucocyte recruitment at the endothelium surface. PECAM-1 and VE-cadherin act to form intercellular junctions that are crucial for maintaining a continuous endothelium and so loss of these cell–cell contacts will inevitably lead to loss of tissue integrity, increased permeability and endothelial dysfunction. In this study, loss of PECAM-1 and VE-cadherin cell surface abundance was identified in response to whole bacteria, whereas previous studies have used recombinant gingipains to show cleavage of endothelial cell surface proteins including N-cadherin and integrin β1 as well as VE-cadherin [24]. Gene expression analysis
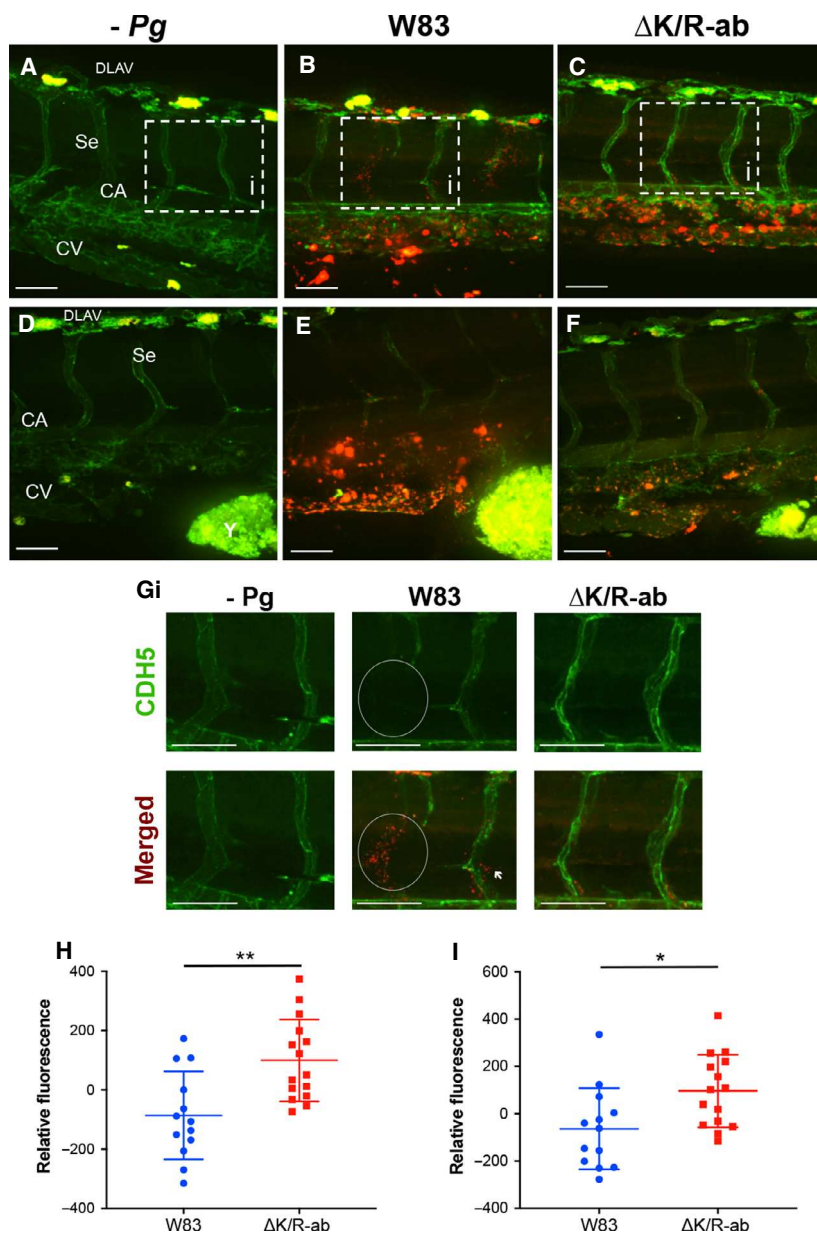
Fig. 7. PECAM-1 expression in an *in vivo* zebrafish embryo systemic infection model. Representative images of spinning disc confocal micrographs showing PECAM-1 expression (green) in the tail region (A–C) and yolk region (D–F) of zebrafish embryos at 24 hpi. Embryos were injected with PBS control (A&D), wild-type W83 *Pg* (red, B&E) or ΔK/R-ab mutant (red, C, F) *n* = 15. Decreased fluorescence in W83 expression was observed in infected segmental vessels, while loss of definition in W83-infected vessels is clearer than in caudal vein and artery. Loss of PECAM-1 expression is exemplified in high-magnification images of the caudal vein showing PBS controls (Gi, top), W83-infected (Gi, middle) and ΔK/R-ab-infected (Gi, lower) embryos and in the intersegmental vessels which show a marked loss of PECAM-1 fluorescence (green) when colocalised with red-labelled W83 (Gii, circled areas). W83 can also be observed in the tissues having traversed the vasculature (Gii, white arrows). Image analysis showed significantly decreased normalised median fluorescence values and therefore PECAM-1 expression in both the tail (H) and caudal vein (I) between zebrafish embryo infected with W83 and ΔK/R-ab *Pg* (**$P < 0.01$, ***$P < 0.001$, Student's *t*-test; data are means ± SD of 3 pooled independent biological experiments (*n* = 3) with 5 technical repeats per experiment). CA, caudal artery; CV, caudal vein; DLAV, dorsal longitudinal anastomotic vessel; Se, intersegmental vessels; Y, yolk sac. Scale bar A–G = 40 μm.
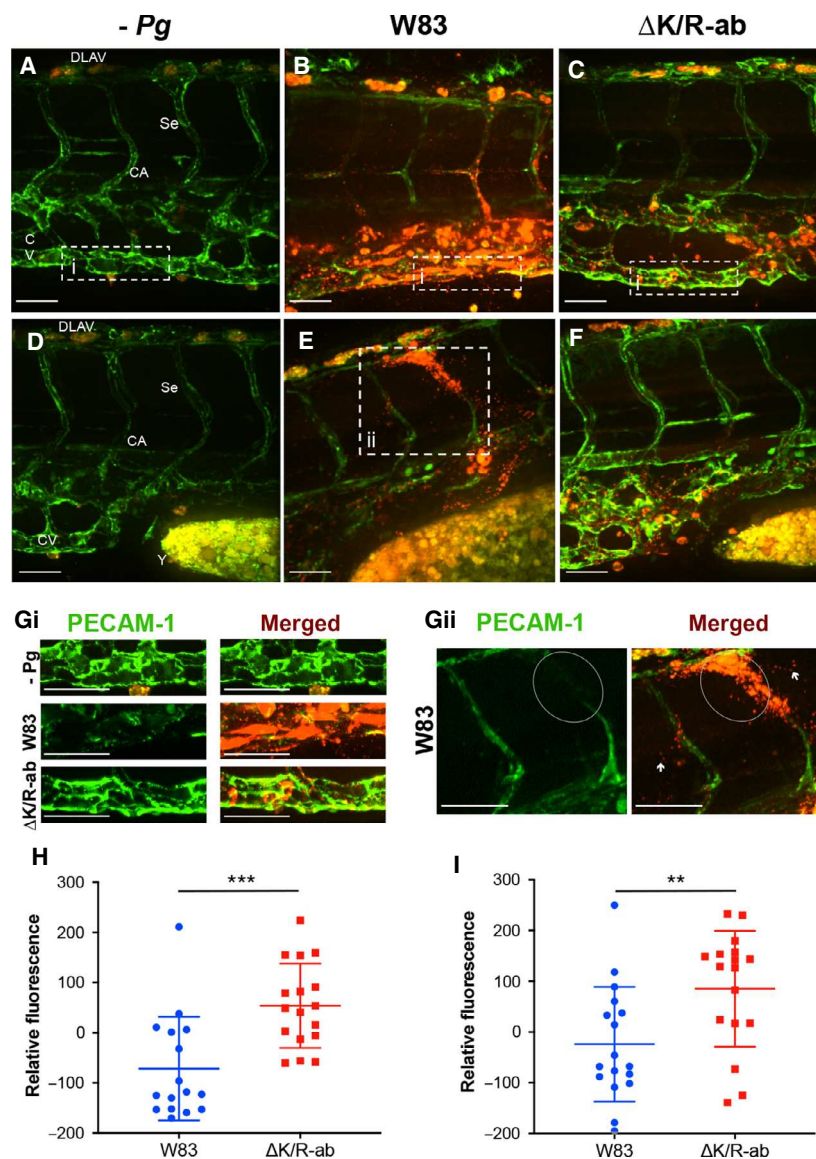
showed no change in expression levels of PECAM-1 or VE-cadherin as well as other inflammatory cytokines (CCL2, CXCL8 and ICAM-1) in response to infection with either wild-type W83 or ΔK/R-ab *Pg*, confirming that loss of cell surface protein was due to protein cleavage and not altered gene transcription. Interestingly, our gene expression data are in contrast to those reported by others who have observed increased gene expression for CCL2 (formally MCP-1) by HUVEC in response to *Pg* strain 381 [42] and ICAM-1 by E.A.hy926 cells (an endothelial/epithelial hybrid cell line) or HUVEC upon infection with *Pg* strain ATCC33277 or W83, respectively [43,44], which may be due to bacterial strain differences or to use of cell lines or endothelial cells derived from large compared with microvascular vessels.

In vitro generated data using monolayer endothelium provide valuable information, but these experiments lack conditions such as flow, shear stress and presence of other cells that are important when examining systemic infection. We therefore set about confirming the *in vitro* data using our zebrafish *Pg* infection model [27]. Zebrafish have been extensively used for host–pathogen interactions as well as for cardiovascular studies [45] and have several advantages over murine models such as transparency and availability of fluorescently tagged proteins that allow for real-time analysis of cell–cell interactions. Moreover,

Fig. 8. VE-cadherin (CDH5) expression in an *in vivo* zebrafish embryo systemic infection model. Representative images of spinning disc confocal micrographs showing VE-cadherin expression (green) in the tail region (A–C) and yolk region (D–F) of zebrafish embryos at 24 hpi. Embryos were injected with PBS control (A, D), wild-type W83 *Pg* (red, B, E) or ΔK/R-ab mutant (red, C, F) *n* = 12. Decreased VE-cadherin fluorescence when colocalised with W83 was observed in infected segmental vessels and caudal vein. The loss of VE-cadherin expression is exemplified in high-magnification images from A, B and C showing PBS controls (Gi, left), W83-infected (Gi, middle) and ΔK/R-ab-infected (Gi, right) intersegmental vessels. Image analysis showed significantly decreased normalised median fluorescence values and therefore VE-cadherin expression in both the tail (G) and caudal vein (H) between zebrafish embryo infected with W83 and ΔK/R-ab mutant *Pg* (*$P < 0.05$, **$P < 0.01$, Student's *t*-test, and data are means ± SD of 3 pooled independent biological experiments (*n* = 3) with 4 technical repeats per experiment). CA, caudal artery; CV, caudal vein; DLAV, dorsal longitudinal anastomotic vessel; Se, intersegmental vessels; Y, yolk sac. Scale bar A-G = 40 μm.

the close homology between numerous zebrafish and human innate immune and cardiovascular-associated molecules means that this *in vivo* model system is also ideally placed to examine pathogen-mediated host responses that may impact on CVD risk. We previously showed that zebrafish present with oedema upon infection with wild-type but not the ΔK/R-ab gingipain-null mutant [27] and given our *in vitro* data on gingipain-dependent endothelial cell adhesion molecule degradation we hypothesised that gingipains would be responsible for cleavage of these molecules *in vivo* leading to vascular permeability. Using genetically engineered zebrafish whereby PECAM-1 or VE-cadherin

was fluorescently labelled, we observed, for the first time, *in vivo Pg*-mediated loss of fluorescence upon infection with wild-type (W83) but not with the gingipain-null mutant strain, indicating gingipain-dependent degradation of these molecules. Loss of PECAM-1 and VE-cadherin on the endothelium was most evident when colocalised with W83 *Pg* and was apparent in several vascular regions of the zebrafish indicating that infection is widespread and that *Pg* adhesion and gingipain-mediated protein degradation are not confined to specific vascular beds. Even more important was that loss of adhesion molecule abundance was associated with increased vascular permeability as
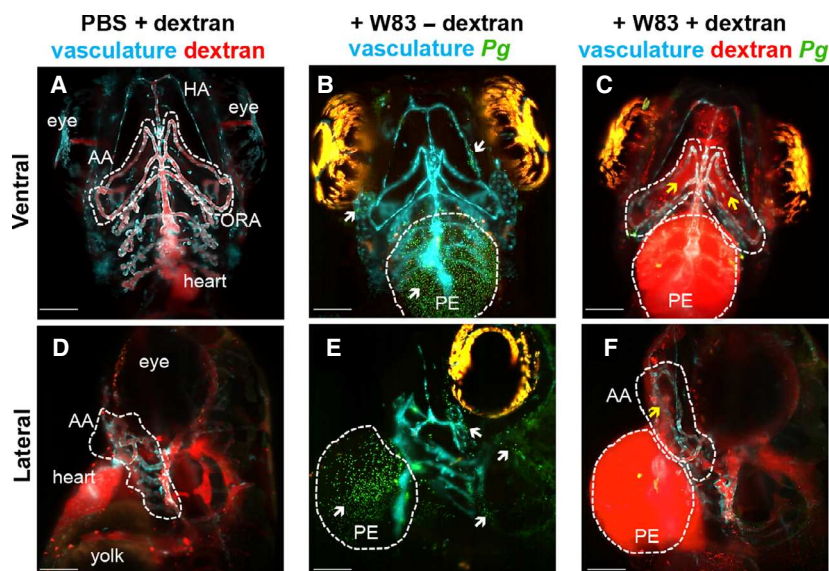
Fig. 9. *Pg* W83 infection increases vascular permeability in zebrafish embryos. Representative maximum intensity Z projection microangiography of PBS-injected (A, D) or fluorescein-stained wild-type W83 *Pg*-infected (green, B, C, E, F) zebrafish embryos with cyan-labelled vasculature before (B, E) and after red fluorescent dextran injection (A, C). Upper panels show ventral view and lower panels lateral view. White arrows in panels B&E indicate W83 within blood vessels, tissues and oedematous heart. Dashed lines in A, C, D and F outline the aortic arches (AA) and opercular artery (ORA) vascular regions. Yellow arrows in C and F point to regions demonstrating dextran leakage from the vasculature into the tissues. Data are representative of $n = 3$ independent biological experiments. HA, hypobranchial artery; PE, pericardial oedema. Scale bar = 100 μm.

determined by dextran vascular leakage, signifying loss of endothelium integrity and vascular damage, both implicated in the pathogenesis of cardiovascular disease [46].

Several *in vivo* studies using murine experimental models, in particular the hyperlipidaemic ApoE(null) mice, have shown that *Pg* infection directly influences atherosclerotic lesion formation or development [47,48] and several mechanisms have been suggested. However, visualising bacterial–host interactions at a cellular and even protein level are not possible in these models. To our knowledge, this is the first time that the effects of systemic *Pg* infection at the cellular level, *in vivo*, have been reported and our data clearly point to a role for *Pg* in mediating vascular damage. At present, it is unknown whether *Pg* acts as an initiating event, where it could be speculated that *Pg*-mediated endothelial cell damage leads to the exposure of the underlying vascular connective tissue leading to localised platelet activation and leucocyte recruitment. However, it could also be speculated that *Pg* acts to exacerbate the disease process by negatively modulating the immune response. Clearly, further studies are warranted to decipher the precise role of *Pg* in CVD.

As with most *in vivo* experimental infection models, animals (mice or zebrafish) are systemically inoculated with high numbers of bacteria, much more than would be observed in humans, and it could be argued that these studies are therefore not completely physiologically relevant. However, it should be noted that many cardiovascular diseases are long-term, chronic conditions where the disease manifests over long periods with repeat exposure to transient levels of one if not several aetiological agents. Replicating this experimentally *in vivo* is extremely challenging and would require repeat low-dose inoculation or a long time frame, giving raise to ethical concerns over animal distress as well as experimental cost. Current, *in vivo* infection strategies aim to provide key information that collectively points to significant risk factors within the full knowledge of their limitations. In this regard, zebrafish provide clear benefits as an *in vivo* model to examine systemic host–pathogen interactions, and our data significantly add to others in implicating *Pg* in vascular pathogenicity. There is now an appreciation that many bacterial-mediated diseases are polymicrobial in nature, with periodontitis being a case in point where it is considered that several organisms within the subgingival plaque drive pathogenesis rather than one organism in isolation. It is therefore likely that other oral bacteria contribute to systemic disease. Indeed, in the oral context, studies have shown significant impacts on

the functional behaviour of *Pg* when in the presence of other oral microbes such as *Tannerella forsythia* or *Fusobacterium nucleatum* [49] and it will be important to determine whether other microbes affect disease progression. Nevertheless, this study provides crucial evidence for the role of *Pg*, and gingipains in particular, in affecting endothelial function, reaffirming the likely role or oral microbes in influencing systemic disease outcomes.

Materials and methods

P. gingivalis strains and culture

Wild-type strains W50, ATCC33277 and W83, as well as clinical strain A245Br, were maintained on Fastidious Anaerobe (FA) agar plates (NeoGen, Ayr, UK) supplemented with 5% v/v oxalated horse blood (Oxoid, Basingstoke, UK). Isogenic gingipain-deficient mutant $kgp\Delta598$-1732::Tc^R $rgpA$-::Cm^R $rgpB\Delta410$-507::Em^R (ΔK/R-ab) was grown on blood FA plates supplemented with 1 µg·mL^{-1} tetracycline and 5 µg·mL^{-1} erythromycin. Liquid cultures were maintained in either Schaedler (BTL Ltd., èódź, Poland) or brain–heart infusion broth (Oxoid) supplemented with 0.5 % yeast extract, 250 µg·mL^{-1} cysteine, 1 mg·mL^{-1} haemin and 1 mg·mL^{-1} vitamin K (Oxoid). Both liquid and agar cultures were incubated at 37 °C in an anaerobic chamber with an atmosphere of 80% N_2, 10% CO_2 and 10% H_2. For use in experiments, strains were grown as liquid cultures anaerobically overnight, adjusted to an optical density (OD$_{600}$) equal to 0.1 and cultured until late log phase. Bacteria were then harvested by centrifugation at 8000 *g* for 3 min, washed with PBS and resuspended at the required density. For zebrafish experiments, bacteria were resuspended in PBS at 5×10^9 CFU·mL^{-1} for microinjection.

Endothelial cell culture

Human primary coronary artery endothelial cells (HCAEC, purchased from the American Tissue Culture Collection) and human primary microvascular endothelial cells (HDMEC, purchased from PromoCell, Heidelberg, Germany) were maintained in MV medium containing MV supplement medium (PromoCell®), while immortalised human dermal microvascular endothelial cells (HMEC-1 provided by F.J. Candal, Centers for Disease Control and Prevention, Atlanta, GA) were grown in MCDB131 (Fisher Scientific, Loughborough, UK) supplemented with 10 ng·mL^{-1} epidermal growth factor (Sigma-Aldrich, Poole, UK), 1 µg·mL^{-1} hydrocortisone (Sigma), 10% v/v fetal calf serum (Thermo Fisher Scientific, Loughborough, UK) and 2 mM L-glutamine (Sigma-Aldrich). All cells were cultured at 37 °C, 5% CO_2 in a humidified atmosphere.

Animals

Zebrafish maintenance and experimental work were carried out in accordance with UK Home Office regulations and UK Animals (Scientific Procedures) Act 1986 and EU directive 2010/63/EU under Project Licence P1A4A7A5E using zebrafish embryos under 5 days postfertilisation (dpf). Nacre wild-type, VE-cadherin transgenic *tg(cdh5$^{ubs8-/-}$;cdh5TS)*, PECAM-1 transgenic *tg(fli1a:PECAM1-EGFP)sh524* and *tg(fli1a:mTurquoise2)sh321* embryos were maintained in E3 medium at 30 °C according to standard protocols. Anaesthesia of zebrafish larvae was achieved by adding 0.16 mg·mL^{-1} tricaine (Sigma-Aldrich) to E3 medium, while addition of 0.3 mg·mL^{-1} tricaine was used for euthanasia.

Generation of zebrafish transgenic lines

Tg(fli1a:PECAM1-EGFP)sh524 was generated via injection of pTol2-fli1a-pecam1-EGFP according to standard protocols. *Tg(fli1a:mTurquoise2)sh321* was generated by PCR amplifying the coding sequence of *mTurquoise2* from pmTQ21-C1, a kind gift of Joachim Goedhart (University of Amsterdam), using the following primers 5′-ggccggatc-catggtgagcaagggcgag-3, 5′-ggccctcgagttacttgtacagctcgtc′-3′ and cloning into the BamHI/XhoI sites of pME-MCS2 [50] to generate pME-mTurquoise2. The pFli1a:mTurquoise2-SV40pA construct was generated using the Tol2kit via standard methods and the following components: *fli1a* enhancer/promoter, pDestTol2-pA2, pME-mTurquoise2 and p3E-SV40pA, and injected into embryos alongside *Tol2* mRNA at 25 pg·nL^{-1}.

Endothelial cell invasion quantification and visualisation

Antibiotic protection endothelial cell invasion assays were performed as described in Naylor *et al.* [51], with modification. HCAEC, HDMEC or HMEC-1 cells were seeded at 2×10^5 cells per well in a 24-well plate and cultured to confluence. Cell monolayers were washed with PBS and blocked for 1 h with 2% bovine serum albumin (BSA; Sigma-Aldrich) in cell culture medium. Endothelial cells were infected with *Pg* strains (ATCC33277, W83, W50 or A245Br) at a multiplicity of infection (MOI) of 100 in cell culture medium and incubated for 90 min at 37 °C, 5% CO_2. Serial dilutions were carried out to determine viable counts through colony-forming units (CFUs). Nonadhered bacteria were removed with PBS and the cell-adherent bacteria killed by incubation with 200 µg·mL^{-1} metronidazole (Sigma-Aldrich) for 1 h at 37 °C, 5 % CO_2. Cells were then washed with PBS, lysed with dH$_2$O, scraped, serially diluted on FA plates and incubated anaerobically for 3 days. CFUs were enumerated to determine the total

number of invading bacteria, expressed as a percentage of the viable count of the initial inoculum.

To visualise *Pg* invasion, HMEC-1 cells were grown overnight on 4-well glass-bottom culture chambers (Sarstedt AG, Nümbrecht, Germany). *Pg* W83 was fluorescently labelled by re-suspension in 0.4 µg·mL^{-1} 5-(and-6)-carboxyfluorescein, succinimidyl ester (5(6)-FAM, SE) (excitation 494 nm, emission 518 nm) (Thermo Fisher Scientific) in PBS for 15 min with shaking at 4 °C. FAM-labelled *Pg* were further biotinylated by diluted in 0.3 mg·mL^{-1} 6-((biotinoyl)amino)hexanoic acid, succinimidyl ester (Thermo Fisher Scientific) in PBS and incubated for 30 min and then resuspended in nonsupplemented MCDB medium. FAM-biotinylated *Pg* were used for invasion (MOI 1000) into HMEC-1 cells for 1 h at 37 °C, 5% CO_2. HMEC-1 cells were fixed with 4% paraformaldehyde (Sigma-Aldrich) for 20 min, washed and blocked with 10% v/v FCS in PBS for 5 min. Alexa Fluor 647®-conjugated streptavidin (excitation 650 nm, emission 655 nm) (Thermo Fisher Scientific) 5 µg·mL^{-1} in PBS containing 10% v/v FCS was incubated with the cells for 45 min at 37 °C, 5% CO_2. After washing, nuclei were counterstained with 7.5 µg·mL^{-1} Hoechst® (excitation 350 nm, emission 461 nm) (Thermo Fisher Scientific) for 10 min, rinsed and the endothelial plasma membrane stained with 5 µg·mL^{-1} wheat germ agglutinin (WGA) (excitation 555 nm, emission 565 nm) (Thermo Fisher Scientific) for 10 min at 37 °C. Chamber slides were analysed using a Zeiss LSM 880 inverted Axio Imager and AiryScan confocal microscope. Images were processed using AiryScan® processing (Zeiss, Oberkochen, Germany), and composite and orthogonal views were created using FIJI® software (National Institute of Health, Bethesda, MD, USA).

Endothelial cell permeability

Endothelial monolayer permeability was measured using a Transwell assay system. Millicell® cell culture inserts (Merck Millipore, Watford, UK) were fibronectin-coated (10 µg·mL^{-1}) prior to seeding with HDMEC that were cultured until confluent. *Pg* W83 were treated with KYT-1 or KYT-36 (2 µM; Peptides International, Louisville, KY, USA) to inhibit gingipain activity as previously described [28]. HDMEC were infected in the absence or presence of *Pg* W83 (with or without inhibitors) at a MOI of 1000 for 1.5 h at 37 °C in nonsupplemented MV medium. Bacteria were removed, inserts transferred to a new 12-well plate with 500 µL supplemented MV medium and 450 µL of MV supplemented medium added to the apical compartment of the insert together with 70 kDa fluorescent-labelled dextran, a molecular weight that does not readily pass through a confluent endothelial monolayer (Thermo Fisher Scientific; final concentration of 65 µg·mL^{-1}). Dextran leakage through the cell monolayer from apical compartment of the insert to the bottom well was monitored for up to 5 h by measuring the fluorescence intensity (excitation 494 nm,

emission 521 nm; Tecan Ltd, Männedorf, Switzerland) of 250 µL medium aspirated from the bottom well; 250 µL of fresh medium was added to the bottom well for further readings. Inserts without cells were used as control wells.

In vitro PECAM-1 and VE-cadherin cell adhesion protein expression

In vitro cell adhesion protein expression was analysed using flow cytometry and immunofluorescence microscopy. For flow cytometric analysis, HMEC-1 and HDMEC were seeded at 4×10^5 cells per well, cultured until confluent, rinsed and infected with MOI 1000 W83 or ΔK/R-ab *Pg* in nonsupplemented medium for 1 h. Addition of medium only was used as a control. Cells were washed, removed using 0.02% EDTA (Sigma-Aldrich) for 20 min, centrifuged and resuspended in 100 µL FACS buffer (0.1 % BSA and 0.1 % sodium azide in PBS). For PECAM-1 (CD31) expression, 0.06 µg per test of PE-Cyanine7-conjugated anti-human PECAM-1 (Clone MW59; Thermo Fisher Scientific) or its matching conjugated IgG control (IgG2254 Isotype Control; Thermo Fisher Scientific) was added and cells incubated for 45 min on ice. For VE-cadherin (CD144), 0.25 µg per reaction anti-human VE-cadherin antibody (Clone 123413, R&D Systems, Minneapolis, MN, USA) or IgG isotype control (Clone 11711, R&D Systems) was incubated for 45 min on ice, supernatant was removed and Alexa Fluor® 488 goat anti-mouse antiserum (Abcam, Cambridge, UK) diluted at 1 : 100 in FACS buffer was added for 30 min on ice. Cells were washed and resuspended in 300 µL FACS buffer, and single-colour sample analysis was carried out using a LSR II flow cytometer (BD Biosciences, San Jose, CA, USA) for PECAM1 and FACSCalibur flow cytometer (BD Biosciences) for VE-cadherin analysis. The cell viability dye, TO-PRO-3® (1 mg·mL^{-1}, Thermo Fisher Scientific), was added to each sample before analysis. Cell populations were gated using forward scatter (FSC) and side scatter (SSC) voltages and TO-PRO-3-positive cells excluded from the analysed population. Five thousand viable cells were collected for HDMEC analysis, while 10 000 live cells were collected for HMEC-1 analysis. Threshold for positively fluorescent cells was set using isotype-matched controls, and data were analysed using FlowJo software (BD Biosciences). The normalised median fluorescence index (nMFI) was calculated by dividing the median fluorescence intensity of the positive samples by that of the IgG controls.

For immunofluorescence microscopy, fibronectin-coated (10 µg·mL^{-1}) glass coverslips were seeded with 5×10^4 endothelial cells. *Pg* was stained with 5 µM Red CMTPX CellTracker® (Thermo Fisher Scientific) and diluted to an MOI 1000 in nonsupplemented cell culture medium to infect primary and immortalised endothelial cells. Cells were washed with PBS, fixed in 3.7% formalin for 10 min at room temperature, washed again and blocked for 1 h

with blocking buffer (2% BSA, 5% goat serum v/v in PBS). For VE-cadherin staining, the cells were incubated overnight at 4 °C with 3 µg·mL^{-1} mouse anti-human VE-cadherin (Clone # 123413, R&D Systems) in blocking buffer, or with mouse IgG1 isotype control (Clone P3.6.2.8.1, R&D Systems) at the same concentration. Following incubation, slides were washed with PBS and incubated with 1 µg·mL^{-1} Alexa Fluor 488 goat anti-mouse IgG (H + L) secondary antibody for 1 h. Cells were rinsed again, mounted in ProLong™ Diamond Antifade Mountant containing 4',6-diaminidine-2'-phylindole dihydrochloride (DAPI) (Thermo Fisher Scientific) and imaged using a Zeiss Axiovert 200M inverted fluorescence microscope with an integrated high-resolution digital camera (AxioCam MRm; Zeiss) with AxioVision 4.6 software (Zeiss). For PECAM-1 staining, cells were blocked with 2.5% BSA in PBS for 40 min and fixed in 2% paraformaldehyde for 20 min at room temperature. Cells were then washed in PBS and stained with PE-Cy7 conjugated anti-human PECAM-1 antibody (Clone WM59, BD Biosciences) for 40 min at room temperature. Nuclei were stained for 5 min with 5 µg·mL^{-1} DAPI (Sigma-Aldrich), washed, mounted ProLong Diamond Antifade Mountant (Thermo Fisher Scientific) and left to set overnight. Images were captured using a Nikon A1 confocal microscope.

In vitro gene expression analysis

Quantitative reverse transcription polymerase chain reaction (qRT–PCR) was used to analyse mRNA expression of endothelial immune molecules. HMEC-1 and HDMEC were seeded at 4×10^5 cells per well and cultured until confluent. Cells were either infected with *P. gingivalis* W83 or ΔK/R-ab mutant at a MOI 100 for 4 h, and unstimulated or TNFα-stimulated (25 ng·mL^{-1}) cells were used as controls. Total RNA extraction was carried out using ISOLATE II RNA Mini Kit (Bioline, Meridian Bioscience Inc., Cincinnati, OH, USA) according to the manufacturer's instructions and RNA measured by NanoDrop (Thermo Fisher Scientific). High-Capacity cDNA Reverse Transcription Kit (Thermo Fisher Scientific) was used to produce cDNA and qPCR performed using Qiagen Rotor-Gene (Qiagen, Hilden, Germany). Reactions consisted of 5 µL of TaqMan® qPCR BioProbe Blue Master Mix (PCR Biosystems, London, UK), 3.5 µL RNase-free water, 0.5 µL human β-2-microglobulin (B2M) as an endogenous reference control (VIC/MGB Probe, Thermo Fisher Scientific), 0.5 µL target primer and 0.5 µL cDNA. Target primers used were PECAM-1 (Hs01065279_m1), VE-cadherin (Hs00901465_m1), CXCL8 (Hs00174103_m1), CCL2 (Hs00234140_m1) and ICAM-1 (Hs0014932_m1) (Thermo Fisher Scientific). All samples were run in triplicate; control samples excluded cDNA. The threshold cycle (Ct) for each test gene was normalised against their respective reference

controls. Fold change in expression relative to unstimulated cells was calculated with ΔC_t values of the sample and reference gene using the formula $2^{-\Delta\Delta C_t}$.

In vivo PECAM-1 and VE-cadherin cell adhesion protein expression

Tg(fli1a:PECAM1-EGFP)sh524 and *Tg(cdh5ubs8-/-;cdh5TS)* transgenic zebrafish were outcrossed with nacre zebrafish. Embryos were dechorionated and green fluorescent protein (GFP)-positive embryos selected at 1 dpf using a fluorescent dissecting microscope (Zeiss Axio Zoom.V16 fitted with an HXP 200C Illuminator and a Zeiss Axiocam 503 monocamera). Zebrafish embryos at 30 hpf were anaesthetised using tricaine (0.02% (w/v) 3-amino benzoic acid ester tricaine/MS-322 (Sigma-Aldrich), positioned in a solution of 3% (w/v) methylcellulose (Sigma-Aldrich) in E3 medium and 2 nL (5×10^4 CFU) of 5 µM Red CMPTX (CellTracker™, Thermo Fisher Scientific) stained W83 or ΔK/R-ab *Pg* were injected systemically using a microcapillary needle (Scientific Laboratory Supplies) via direct microinjection into the Duct of Cuvier (the common cardinal vein); PBS was used as control. Live imaging of anaesthetised fish (5 zebrafish embryos per group) was carried out 24 h postinfection (hpi) using a spinning disc confocal microscope (PerkinElmer UltraVIEW VoX, PerkinElmer Inc., Waltham, MA, USA) running on an inverted Olympus IX81 motorised microscope. 488-nm and 561-nm lasers were used to visualise fluorescent PECAM-1 or CDH5/VE-cadherin (green) and *Pg* bacteria (red) in zebrafish embryos. Micrographs were captured in two areas of the tail, adjacent to the cloaca (closer to the yolk) and 4 vessels further away from the cloaca (closer to the tip of the tail) using Volocity® software (Quorum Technologies Inc., Puslinch, Ontario, Canada). Quantification of relative GFP fluorescence intensity (pixel value) was performed by batch processing of maximum intensity z projection of micrographs of whole images in the yolk and tail region using an adjusted script on FIJI® Macros plug-in.

In vivo vascular permeability

Zebrafish *Tg(fli1a:mTurquoise2)sh321* embryos were infected at 2 dpf with FAM-labelled *Pg* W83, ΔK/R-ab or PBS as a control, into the common cardinal vein. Embryos with a functional circulation at 24 hpi were anaesthetised and injected into the posterior cardinal vein (PCV) with 2 nL of 1 mg·mL^{-1} tetramethylrhodamine dextran (2×10^6 kDa, Thermo Fisher Scientific). Microangiogram images were acquired within an hour postdextran injection. Real-time changes in vascular integrity were measured in response to *Pg* W83 infection using light sheet microscopy (Z1, Zeiss) with lasers 445-24, 488-30 and 561-20 with LSB 445/514/640.

Statistical analysis

All data presented are from at least 3 independent experiments (unless specified). Results are expressed as the mean $\pm$ standard deviation (SD) except for flow cytometry data where the nMFI (normalised median fluorescence index) was used. Normality was determined using Kolmogorov–Smirnov analysis. The differences between two groups were assessed using either Student's *t*-test or Mann–Whitney *U*-test, while the differences between group data were assessed using one-way ANOVA followed by either Tukey's or Dunn's post hoc multiple comparison test depending on the nature of the data (parametric or non-parametric). All tests were carried out using GraphPad Prism v8.2 (GraphPad, San Diego, CA, USA), and statistical significance was assumed at $P < 0.05$.

Acknowledgements

Conflict of interest

The authors declare no conflict of interest.

Author contributions

CM, GPS, JP, RNW and MW conceived, designed the research and planned experiments. CF, YC and MW performed the experiments. CF, MW, GPS and CM analysed the data, conducted statistical analysis and interpreted the results. CF, MW and CM wrote the manuscript draft, and further editing was performed by GPS, CM, JP and RNW.

References

1 Tonetti MS & Van Dyke TE (2013) Periodontitis and atherosclerotic cardiovascular disease: consensus report of the Joint EFP/AAP Workshop on Periodontitis and Systemic Diseases. *J Periodontol* **84**, S24–S29.

2 Fiehn NE, Larsen T, Christiansen N, Holmstrup P & Schroeder TV (2005) Identification of periodontal pathogens in atherosclerotic vessels. *J Periodontol* **76**, 731–736.

3 Mikuls TR, Payne JB, Yu F, Thiele GM, Reynolds RJ, Cannon GW, Markt J, McGowan D, Kerr GS, Redman RS *et al.* (2014) Periodontitis and *Porphyromonas gingivalis* in patients with rheumatoid arthritis. *Arthritis Rheumatol* **66**, 1090–1100.

4 Saremi A, Nelson RG, Tulloch-Reid M, Hanson RL, Sievers ML, Taylor G, Shlossman M, Bennett PH, Genco R & Knowler WC (2005) Periodontal disease and mortality in type 2 diabetes. *Diabetes Care* **28**, 27–32.

5 Olsen I, Taubman MA & Singhrao SK (2016) *Porphyromonas gingivalis* suppresses adaptive immunity in periodontitis, atherosclerosis, and Alzheimer's disease. *J Oral Microbiol* **8**, 33029.

6 Friedewald VE, Kornmam KS, Beck JD, Genco R, Goldfine A, Libby P, Offenbacher S, Ridker PM, Van Dyke TE & Roberts WC (2009) The American Journal of Cardiology and Journal of Periodontology editors' consensus: periodontitis and atherosclerotic cardiovascular disease. *Am J Cardiol* **104**, 59–68.

7 Darveau RP (2010) Periodontitis: a polymicrobial disruption of host homeostasis. *Nat Rev Microbiol* **8**, 481–490.

8 Lamont RJ, Koo H & Hajishengallis G (2018) The oral microbiota: dynamic communities and host interactions. *Nat Rev Microbiol* **16**, 745–759.

9 Hajishengallis G, Darveau RP & Curtis MA (2012) The keystone-pathogen hypothesis. *Nat Rev Microbiol* **10**, 717–725.

10 How KY, Song KP & Chan KG (2016) *Porphyromonas gingivalis*: an overview of periodontopathic pathogen below the gum line. *Front Microbiol* **7**, 53.

11 Potempa J, Sroka A, Imamura T & Travis J (2003) Gingipains, the major cysteine proteinases and virulence factors of *Porphyromonas gingivalis*: structure, function and assembly of multidomain protein complexes. *Curr Protein Pept Sci* **4**, 397–407.

12 Bahrani-Mougeot FK, Paster BJ, Coleman S, Ashar J, Barbuto S & Lockhart PB (2008) Diverse and novel oral bacterial species in blood following dental procedures. *J Clin Microbiol* **46**, 2129–2132.

13 Schenkein HA & Loos BG (2013) Inflammatory mechanisms linking periodontal diseases to cardiovascular diseases. *J Clin Periodontol* **40**, S51–S69.

14 Loos BG (2005) Systemic markers of inflammation in periodontitis. *J Periodontol* **76**, 2106–2115.

15 Castillo DM, Sánchez-Beltrán MC, Castellanos JE, Sanz I, Mayorga-Fayad I, Sanz M & Lafaurie GI (2011) Detection of specific periodontal microorganisms from bacteraemia samples after periodontal therapy using molecular-based diagnostics. *J Clin Periodontol* **38**, 418–27.

16 Mougeot JLC, Stevens CB, Paster BJ, Brennan MT, Lockhart PB & Mougeot FKB (2017) *Porphyromonas gingivalis* is the most abundant species detected in coronary and femoral arteries. *J Oral Microbiol* **9**, 1281562.

17 Oliveira FA, Forte CP, Silva PG, Lopes CB, Montenegro RC, Santos AK, Sobrinho CR, Mota MR, Sousa FB & Alves AP (2015) Molecular analysis of oral bacteria in heart valve of patients with cardiovascular disease by real-time polymerase chain reaction. *Medicine* **94**, e2067.

18 Dorn BR, Dunn WA & Progulske-Fox A (1999) Invasion of human coronary artery cells by periodontal pathogens. *Infect Immun* **67**, 5792–5798.

19 Deshpande RG, Khan MB & Genco CA (1998) Invasion of aortic and heart endothelial cells by *Porphyromonas gingivalis*. *Infect Immun* **66**, 5337–5343.

20 Nassar H, Chou HH, Khlgatian M, Gibson FC, Van Dyke TE & Genco CA (2002) Role for fimbriae and lysine-specific cysteine proteinase gingipain K in expression of interleukin-8 and monocyte chemoattractant protein in *Porphyromonas gingivalis*-infected endothelial cells. *Infect Immun* **70**, 268–276.

21 Takahashi Y, Davey M, Yumoto H, Gibson FC & Genco CA (2006) Fimbria-dependent activation of pro-inflammatory molecules in *Porphyromonas gingivalis*-infected human aortic endothelial cells. *Cell Microbiol* **8**, 738–757.

22 Walter C, Zahlten J, Schmeck B, Schaudinn C, Hippenstiel S, Frisch E, Hocke AC, Pischon N, Kuramitsu HK, Bernimoulin JP *et al.* (2004) *Porphyromonas gingivalis* strain-dependent activation of human endothelial cells. *Infect Immun* **72**, 5910–5918.

23 Yun PL, Decarlo AA, Chapple CC & Hunter N (2005) Functional implication of the hydrolysis of platelet endothelial cell adhesion molecule 1 (CD31) by gingipains of *Porphyromonas gingivalis* for the pathology of periodontal disease. *Infect Immun* **73**, 1386–1398.

24 Sheets SM, Potempa J, Travis J, Casiano CA & Fletcher HM (2005) Gingipains from *Porphyromonas gingivalis* W83 induce cell adhesion molecule cleavage and apoptosis in endothelial cells. *Infect Immun* **73**, 1543–1552.

25 Dejana E, Orsenigo F & Lampugnani MG (2008) The role of adherens junctions and VE-cadherin in the control of vascular permeability. *J Cell Sci* **121**, 2115–2122.

26 Aghajanian A, Wittchen ES, Allingham MJ, Garrett TA & Burridge K (2008) Endothelial cell junctions and the regulation of vascular permeability and leukocyte transmigration. *J Thromb Haemost* **6**, 1453–1460.

27 Widziolek M, Prajsnar TK, Tazzyman S, Stafford GP, Potempa J & Murdoch C (2016) Zebrafish as a new model to study effects of periodontal pathogens on cardiovascular diseases. *Sci Rep* **6**, 36023.

28 Kadowaki T, Baba A, Abe N, Takii R, Hashimoto M, Tsukuba T, Okazaki S, Suda Y, Asao T & Yamamoto K (2004) Suppression of pathogenicity of *Porphyromonas gingivalis* by newly developed gingipain inhibitors. *Mol Pharmacol* **66**, 1599–1606.

29 Privratsky JR & Newman PJ (2014) PECAM-1: regulator of endothelial junctional integrity. *Cell Tissue Res* **355**, 607–619.

30 Yun PL, Decarlo AA & Hunter N (2006) Gingipains of *Porphyromonas gingivalis* modulate leukocyte adhesion molecule expression induced in human endothelial cells by ligation of CD99. *Infect Immun* **74**, 1661–1672.

31 Kozarov EV, Dorn BR, Shelburne CE, Dunn WA & Progulske-Fox A (2005) Human atherosclerotic plaque contains viable invasive *Actinobacillus actinomycetemcomitans* and *Porphyromonas gingivalis*. *Arterioscler Thromb Vasc Biol* **25**, e17–e18.

32 Gaetti-Jardim E, Marcelino SL, Feitosa ACR, Romito GA & Avila-Campos MJ (2009) Quantitative detection of periodontopathic bacteria in atherosclerotic plaques from coronary arteries. *J Med Microbiol* **58**, 1568–1575.

33 Szulc M, Kustrzycki W, Janczak D, Michalowska D, Baczynska D & Radwan-Oczko M (2015) Presence of periodontopathic bacteria DNA in atheromatous plaques from coronary and carotid arteries. *Biomed Res Int* **2015**, 825397.

34 Fitzpatrick RE, Wijeyewickrema LC & Pike RN (2009) The gingipains: scissors and glue of the periodontal pathogen, *Porphyromonas gingivalis*. *Future Microbiol* **4**, 471–487.

35 Rodrigues PH, Reyes L, Chadda AS, Bélanger M, Wallet SM, Akin D, Dunn W & Progulske-Fox A (2012) *Porphyromonas gingivalis* strain specific interactions with human coronary artery endothelial cells: a comparative study. *PLoS One* **7**, e52606.

36 Olsen I & Progulske-Fox A (2015) Invasion of *Porphyromonas gingivalis* strains into vascular cells and tissue. *J Oral Microbiol* **7**, 28788.

37 Lamont RJ, Chan A, Belton CM, Izutsu KT, Vasel D & Weinberg A (1995) *Porphyromonas gingivalis* invasion of gingival epithelial cells. *Infect Immun* **63**, 3878–3885.

38 Pinnock A, Murdoch C, Moharamzadeh K, Whawell S & Douglas CW (2014) Characterisation and optimisation of organotypic oral mucosal models to

study *Porphyromonas gingivalis* invasion. *Microbes Infect* **16**, 310–319.

39 Yamatake K, Maeda M, Kadowaki T, Takii R, Tsukuba T, Ueno T, Kominami E, Yokota S & Yamamoto K (2007) Role for gingipains in *Porphyromonas gingivalis* traffic to phagolysosomes and survival in human aortic endothelial cells. *Infect Immun* **75**, 2090–2100.

40 Deshpande RG, Khan M & Genco CA (1998) Invasion strategies of the oral pathogen *Porphyromonas gingivalis*: Implications for cardiovascular disease. *Invasion Metastasis* **18**, 57–69.

41 Komatsu T, Nagano K, Sugiura S, Hagiwara M, Tanigawa N, Abiko Y, Yoshimura F, Furuichi Y & Matsushita K (2012) E-selectin mediates *Porphyromonas gingivalis* adherence to human endothelial cells. *Infect Immun* **80**, 2570–2576.

42 Choi EK, Park SA, Oh WM, Kang HC, Kuramitsu HK, Kim BG & Kang IC (2005) Mechanisms of *Porphyromonas gingivalis*-induced monocyte chemoattractant protein-1 expression in endothelial cells. *FEMS Immunol Med Microbiol* **44**, 51–58.

43 Mao S, Maeno N, Matayoshi S, Yoshiie K, Fujimura T & Oda H (2004) The induction of intercellular adhesion molecule-1 on human umbilical vein endothelial cells by a heat-stable component of *Porphyromonas gingivalis*. *Curr Microbiol* **48**, 108–112.

44 Xu W, Pan Y, Xu Q, Wu Y, Pan J, Hou J, Lin L, Tang X, Li C, Liu J & *et al.* (2018) *Porphyromonas gingivalis* ATCC 33277 promotes intercellular adhesion molecule-1 expression in endothelial cells and monocyte-endothelial cell adhesion through macrophage migration inhibitory factor. *BMC Microbiol* **18**, 16.

45 Gut P, Reischauer S, Stainier DYR & Arnaout R (2017) Little fish, big data: zebrafish as a model for cardiovascular and metabolic disease. *Physiol Rev* **97**, 889–938.

46 Chistiakov DA, Orekhov AN & Bobryshev YV (2015) Endothelial barrier and its abnormalities in cardiovascular disease. *Front Physiol* **6**, 365.

47 Koizumi Y, Kurita-Ochiai T, Oguchi S & Yamamoto M (2008) Nasal immunization with *Porphyromonas gingivalis* outer membrane protein decreases *P. gingivalis*-induced atherosclerosis and inflammation in spontaneously hyperlipidemic mice. *Infect Immun* **76**, 2958–2965.

48 Velsko IM, Chukkapalli SS, Rivera MF, Lee J-Y, Chen H, Zheng D, Bhattacharyya I, Gangula PR, Lucas AR & Kesavalu L (2014) Active invasion of oral and aortic tissues by *Porphyromonas gingivalis* in mice causally links periodontitis and atherosclerosis. *PLoS One* **9**, e97811.

49 Chukkapalli SS, Easwaran M, Rivera-Kweh MF, Velsko IM, Ambadapadi S, Dai J, Larjava H, Lucas AR & Kesavalu L (2017) Sequential colonization of periodontal pathogens in induction of periodontal disease and atherosclerosis in LDLRnull mice. *Pathogen Dis* **75**, ftx003.

50 Savage AM, Kurusamy S, Chen Y, Jiang Z, Chhabria K, MacDonald RB, Kim HR, Wilson HL, van Eeden FJM, Armesilla AL *et al.* (2019) Tmem33 is essential for VEGF-mediated endothelial calcium oscillations and angiogenesis. *Nat Commun* **10**, 732.

51 Naylor KL, Widziolek M, Hunt S, Conolly M, Hicks M, Stafford P, Potempa J, Murdoch C, Douglas CWI & Stafford GP (2017) Role of OmpA2 surface regions of *Porphyromonas gingivalis* in host-pathogen interactions with oral epithelial cells. *Microbiologyopen* **6**, e00401.